Bericht 186, Institut für Mathematik, TUHH
⊥∀⊥ 1


# ON STRUCTURED PENCILS ARISING IN SONNEVELD METHODS*

JENS-PETER M. ZEMKE†

**Abstract.** The pencils arising in Sonneveld methods, e.g., methods based on the induced dimension reduction (IDR) principle by Sonneveld and van Gijzen, are highly structured and some eigenvalues are known. The other eigenvalues are approximations to eigenvalues of the matrix used to compute the Sonneveld pencil. In [SIAM J. Matrix Anal. Appl. 34(2), 2013, pp. 283–311] we proved that it is possible to purify the characteristic polynomial from the known values by moving them to infinity and to deflate the problem to obtain a smaller pencil that has only the other eigenvalues. Depending on the strategy used to select the known eigenvalues, this may result in large condition numbers or even break down due to a singular pencil. In this paper we prove that there are one-dimensional families of purified and deflated pencils that all have the same eigenvalues. We give a selection scheme to chose a pencil suitable for the stable computation of the wanted eigenvalues.

**Key words.** IDR; Lanczos; Sonneveld pencil; purified pencil; deflated pencil; QZ algorithm; LZ algorithm; LR algorithm; structured pencil.

**AMS subject classifications.** 65F15 (primary); 15A22; 15A18; 65F50.

## 1. Introduction.

In [13] we developed the mathematical theory of an eigensolver based on Sonneveld's and van Gijzen's method of induced dimension reduction (IDR) [36, 29]. In [18] we refined the theory and extended it to its generalization IDRStab [31, 25]. The arising pencils are banded upper Hessenberg/triangular, a property that is destroyed if we use a standard QZ algorithm. Due to the peculiarities of IDR-based methods, some eigenvalues of the pencils are known in advance. We sketch our ideas to reliably compute the other eigenvalues. It turns out that the pencils that are used in [13, 18] to compute the wanted portion of eigenvalues might be numerically unstable, i.e., close to a singular pencil or even non-existent. Our main result in this paper is that it is possible to develop a stable scheme to extract only the unknown eigeninformation by picking an alternate pencil from infinitely many at virtually no extra cost.

### 1.1. Motivation.

In [13] we proved that it is possible to compute eigenvalue approximations based on the induced dimension reduction (IDR) principle. We treated only the prototype IDR($s$) [29] and considered error-free computations apart from a small numerical example. In [18] we extended these ideas to the methods described in [35, 31, 25]. Recent variations of IDR($s$) [18, 34, 19] are based on different basis expansions and on different selection schemes for the known eigenvalues, which can result in almost or exactly singular purified pencils if they are computed as sketched in [13, 18]. We state a particular simple observation we missed in [13] that enables us to come up with families of purified and deflated pencils with varying eigenvalue condition, such that the purification and deflation used in [13, 18] are special instances of the general scheme.

### 1.2. Notation.

We use boldface letters to denote matrices and vectors. The identity matrix of size $n \times n$ is denoted by $\mathbf{I}_n$ with columns by $\mathbf{e}_j$, $1 \leqslant j \leqslant n$, and elements $\delta_{i,j}$, $1 \leqslant i, j \leqslant n$ (Kronecker delta). A zero matrix of size $n \times k$ is denoted by $\mathbf{O}_{n,k}$, a zero column vector of length $k$ by $\mathbf{o}_k$. We omit indices when they are easily deducible from the context. We are interested in the eigenvalues $\lambda$ of the matrix $\mathbf{A} \in \mathbb{C}^{n\times n}$. Column vectors of matrices are denoted by the same letter, e.g., $\mathbf{a}_j \in \mathbb{C}^n$, $1 \leqslant j \leqslant n$, are the columns of $\mathbf{A}$. Scalars are denoted by Greek letters, entries of matrices and vectors are denoted by small Roman letters, e.g., $a_{i,j}$ is the entry of $\mathbf{A}$ in row $i$ and column $j$. Spaces are denoted by calligraphic letters like $\mathcal{S}$, $\mathcal{K}_k$, $\mathcal{G}_j$. Sonneveld methods are related to a set of basis vectors that live in certain spaces $\mathcal{G}_j$. These are denoted by $\mathbf{g}_k \in \mathbb{C}^n$ and are collected in matrices $\mathbf{G}_k \in \mathbb{C}^{n\times k}$,

*Version of July 23, 2014, 12:22.
†Institut für Mathematik E-10, Lehrstuhl Numerische Mathematik, Technische Universität Hamburg-Harburg, D-21073 Hamburg, Germany (zemke@tu-harburg.de).

$1 \leqslant k$. Krylov methods in general, and Sonneveld methods in particular, compute unreduced extended Hessenberg matrices. These are denoted by $\underline{\mathbf{H}}_k \in \mathbb{C}^{(k+1)\times k}$, where the underbar should remind of an additional row vector appended at the bottom of the square upper Hessenberg matrix $\mathbf{H}_k \in \mathbb{C}^{k\times k}$. Sonneveld methods differ from other Krylov subspace methods in constructing additionally upper triangular matrices $\mathbf{U}_k \in \mathbb{C}^{k\times k}$. The Schur complement of the nonsingular matrix $\mathbf{B}$ in the partitioned matrix $\mathbf{A} = \left(\begin{smallmatrix}\mathbf{B} & \mathbf{C}\\ \mathbf{D} & \mathbf{E}\end{smallmatrix}\right)$ is denoted by $\mathbf{A}/\mathbf{B} := \mathbf{E} - \mathbf{D}\mathbf{B}^{-1}\mathbf{C}$, cf. [40, p. 3]. The inclusion and strict inclusion of sets is denoted by $\subseteq$ and $\subset$, respectively. For a linear subspace $\mathcal{S} \subseteq \mathbb{C}^n$, $\mathcal{S}^\perp := \{\mathbf{v} \in \mathbb{C}^n \mid \mathbf{s}^\mathsf{T}\mathbf{v} = 0 \ \forall\ \mathbf{s} \in \mathcal{S}\}$ denotes the annihilator, sometimes called orthogonal complement, of $\mathcal{S}$ in $\mathbb{C}^n$. For reasons stated in [18], we call all transpose-free Lanczos-type methods *Sonneveld methods*.

**1.3. Outline.** In §2 we briefly sketch the origin of Sonneveld pencils and the processes of purification and deflation, for details we refer to [13, 18]. In §3 we remark on possible implementations to compute the eigenvalues of interest of these Sonneveld pencils, and their possible drawbacks. In §4 we present our main result, namely, that a given Sonneveld pencil defines a one-dimensional family of purified pencils and a one-dimensional family of deflated pencils with corresponding families of left and right eigenvectors that are polynomials in the parameter of the pencils, thereby with varying condition numbers of its constant eigenvalues. The deflated family is very simple, it consists of a block-wise diagonal scaling of a particular single deflated pencil. In §5 we sketch how to pick a pencil that has the potential that there exists a method to compute its eigenvalues in a stable manner. In §6 we present a few numerical experiments that show the effectiveness of our approach. We conclude in §7 and give an outlook on the application of the results of §4 to the computation of eigenvectors and to the solution of linear systems.

**2. Sonneveld methods.** In [1] the authors presented a family of Lanczos methods based on a different number of starting vectors for the left and right Krylov subspaces. IDR($s$) is related to a method we call Lanczos($s, 1$) that is based on $s$ left starting vectors and one right starting vector. Let $\mathbf{A} \in \mathbb{C}^{n\times n}$. Skipping over technical details, $ks$ steps of Lanczos($s, 1$) compute, provided no breakdown or deflation occurs, block-biorthogonal bases $\mathbf{Q}_{ks}$, $\widehat{\mathbf{Q}}_{ks}$ of the two Krylov subspaces

$$\begin{aligned}\mathcal{K}_{ks} &:= \mathcal{K}_{ks}(\mathbf{A}, \mathbf{q}) := \mathsf{span}\,\{\mathbf{q}, \mathbf{A}\mathbf{q}, \mathbf{A}^2\mathbf{q}, \ldots, \mathbf{A}^{ks-1}\mathbf{q}\}, \quad \mathbf{q} \in \mathbb{C}^n,\\ \widehat{\mathcal{K}}_k &:= \mathcal{K}_k(\mathbf{A}^\mathsf{H}, \widehat{\mathbf{Q}}) := \mathsf{span}\,\{\widehat{\mathbf{Q}}, \mathbf{A}^\mathsf{H}\widehat{\mathbf{Q}}, \mathbf{A}^{2\mathsf{H}}\widehat{\mathbf{Q}}, \ldots, \mathbf{A}^{(k-1)\mathsf{H}}\widehat{\mathbf{Q}}\}, \quad \widehat{\mathbf{Q}} \in \mathbb{C}^{n\times s},\end{aligned} \tag{2.1}$$

the latter a block Krylov subspace, such that

$$\widehat{\mathbf{Q}}_{ks}^\mathsf{H}\mathbf{A}\mathbf{Q}_{ks} = \mathbf{L}_{ks}, \quad \widehat{\mathbf{Q}}_{ks}^\mathsf{H}\mathbf{Q}_{ks} = \mathbf{I}_{ks}, \quad \mathbf{Q}_{ks}\mathbf{e}_1 = \mathbf{q}, \quad \widehat{\mathbf{Q}}_{ks}\mathbf{I}_{n,s} = \widehat{\mathbf{Q}}, \tag{2.2}$$

where the Lanczos($s, 1$) matrix $\mathbf{L}_{ks} \in \mathbb{C}^{ks\times ks}$ is upper Hessenberg and block tridiagonal with blocks of size $s \times s$. Numerical experiments suggest that when $\widehat{\mathbf{Q}}$ is chosen at random, for larger $s$ the resulting eigenvalue approximations get closer to the approximations obtained by Arnoldi's method [2] started with $\mathbf{q}$. A partial explanation of this phenomenon can be found in [28], a supporting numerical experiment can be found in [18].

Sonneveld ($s = 1$) and Sonneveld & van Gijzen ($s \in \mathbb{N}$) proved that these eigenvalue approximations can be obtained without the need for $\mathbf{A}^\mathsf{H}$ by introducing extra multiplications by $\mathbf{A}$. This follows from the so-called IDR Theorem.

THEOREM 2.1. *Set* $\mathcal{S} := \{\mathbf{v} \in \mathbb{C}^n \mid \widehat{\mathbf{Q}}^\mathsf{H}\mathbf{v} = \mathbf{o}_s\}$. *Define for the* seed values $\mu_1, \ldots, \mu_k \in \mathbb{C}$, $k \in \mathbb{N}$, *the* Sonneveld spaces *[25]*

$$\mathcal{G}_j := M_j(\mathbf{A})\left(\mathcal{K}_n(\mathbf{A}, \mathbf{q}) \cap \widehat{\mathcal{K}}_j^\perp\right), \quad M_j(z) := \prod_{\ell=1}^{j}(z - \mu_\ell), \quad 0 \leqslant j \leqslant k. \tag{2.3}$$

*Then these spaces satisfy the recursion*

$$\mathcal{G}_0 = \mathcal{K}_n(\mathbf{A}, \mathbf{q}), \quad \mathcal{G}_j = (\mathbf{A} - \mu_j\mathbf{I})\mathcal{V}_{j-1}, \quad \mathcal{V}_{j-1} := \mathcal{G}_{j-1} \cap \mathcal{S}, \quad 1 \leqslant j \leqslant k. \tag{2.4}$$

*If no eigenvector lies in* $\mathcal{K}_n(\mathbf{A},\mathbf{q})\cap\mathcal{S}$,

$$\{\mathbf{o}\}=\mathcal{G}_n\subseteq\mathcal{G}_{n-1}\subseteq\cdots\subseteq\mathcal{G}_m\subset\mathcal{G}_{m-1}\subset\cdots\subset\mathcal{G}_j\subset\mathcal{G}_{j-1}\subset\mathcal{G}_1\subset\mathcal{G}_0. \tag{2.5}$$

We reversed the historical development of IDR($s$); the recursion (2.4) came first [36, 29], the characterization in terms of polynomial images of Krylov subspaces came later [24, 25]. The first generation of Sonneveld methods, ignoring IDR [36] and starting with CGS [27] and BiCGStab [33, 32], was based on the explicit computation of the entries of (a certain factorization of) the Lanczos$(1,1)$ matrix and Sonneveld's trick to rewrite the *inner products*. The second, new generation of Sonneveld methods is based on rewriting the *spaces* in a similar manner, which offers more flexibility in deriving new methods. Especially, look-ahead strategies are more easily implemented, as breakdown occurs only at the next level, the selection of appropriate basis vectors.

**2.1. Basis expansions.** The recursion (2.4) is at the heart of Sonneveld methods. We ignore breakdowns and look-ahead and use orthonormalization whenever possible. This gives us $s+1$ orthonormal vectors $\mathbf{g}_1,\ldots,\mathbf{g}_{s+1}$ in $\mathcal{K}_{s+1}(\mathbf{A},\mathbf{q})$ and $s+1$ orthonormal vectors $\mathbf{g}_{j(s+1)+1},\ldots,\mathbf{g}_{(j+1)(s+1)}$ in every $\mathcal{G}_j\setminus\mathcal{G}_{j-1}$, such that we obtain a *generalized Hessenberg decomposition* [13] for $\mathbf{G}_{m+1}=\big(\mathbf{G}_m,\mathbf{g}_{m+1}\big)$, $\mathbf{G}_m=\big(\mathbf{g}_1,\ldots,\mathbf{g}_m\big)$,

$$\mathbf{A}\mathbf{V}_m=\mathbf{A}\mathbf{G}_m\mathbf{U}_m=\mathbf{G}_{m+1}(\underline{\mathbf{H}}_m+\underline{\mathbf{U}}_m\mathbf{D}_m),\quad \mathbf{V}_m=\mathbf{G}_m\mathbf{U}_m, \tag{2.6}$$

where $\mathbf{U}_m\in\mathbb{C}^{m\times m}$ is unit upper triangular, $\underline{\mathbf{U}}_m\in\mathbb{C}^{(m+1)\times m}$ is $\mathbf{U}_m$ with an additional zero row appended at the bottom, $\underline{\mathbf{H}}_m\in\mathbb{C}^{(m+1)\times m}$ is unreduced upper Hessenberg, and $\mathbf{D}_m\in\mathbb{C}^{m\times m}$ is diagonal with $s$ zeros followed by $s+1$ times $\mu_1$, $s+1$ times $\mu_2$ and so forth. In [18] we sketched three different ways to expand the basis; in the forthcoming report [19] we term these methods (in the order of appearance in [18]) *short recurrence IDR* (srIDR), *fast matrix IDR* (fmIDR), and *minimum norm expansion IDR* (mneIDR).

**2.2. Sonneveld pencil & Sonneveld matrix.** The matrices $\mathbf{U}_m$ and $\underline{\mathbf{H}}_m$ have a special structure, we depict a very general structure[1] for $s=2$ and $m=9=3(s+1)$:

$$\mathbf{U}_9=\left(\begin{array}{ccccccccc}\circ&\bullet&\bullet&\bullet&&&&&\\ &\circ&\bullet&\bullet&\bullet&&&&\\ &&\circ&\bullet&\bullet&&&&\\ &&&\circ&\bullet&\bullet&\bullet&\bullet&\\ &&&&\circ&\bullet&\bullet&\bullet&\\ &&&&&\circ&\bullet&\bullet&\\ &&&&&&\circ&\bullet&\bullet\\ &&&&&&&\circ&\bullet\\ &&&&&&&&\circ\end{array}\right),\quad \underline{\mathbf{H}}_9=\left(\begin{array}{ccccccccc}\bullet&\bullet&&&&&&&\\ \circ&\bullet&\bullet&&&&&&\\ &\circ&\bullet&\bullet&&&&&\\ &&\circ&\bullet&\bullet&&&&\\ &&&\circ&\bullet&\bullet&&&\\ &&&&\circ&\bullet&\bullet&&\\ &&&&&\circ&\bullet&\bullet&\\ &&&&&&\circ&\bullet&\bullet\\ &&&&&&&\circ&\bullet\end{array}\right). \tag{2.7}$$

Circles in $\mathbf{U}_9$ depict the unit diagonal elements, circles in $\underline{\mathbf{H}}_9$ depict nonzero elements. Bullets denote elements defined by the Sonneveld method used to compute basis vectors. Elements denoted by bullets in $\mathbf{U}_9$ are used to ensure that the resulting linear combination of $\mathbf{g}$-vectors is in $\mathcal{S}$, we term these elements *Sonneveld coefficients*. As we are only allowed to use vectors that are in the last Sonneveld space $\mathcal{G}_{j-1}$ to compute new vectors in the next Sonneveld space $\mathcal{G}_j$, we can use all $s+1$ vectors in $\mathcal{G}_{j-1}$ in the first step. In the following steps we can also use the vectors in $\mathcal{G}_j\subset\mathcal{G}_{j-1}$. This gives the block shape of the upper triangular $\mathbf{U}_9$. The elements denoted by bullets and circles in $\underline{\mathbf{H}}_9$ correspond to basis transformations in the current $\mathcal{G}_j$; bullets arise form orthogonalization, and circles from normalization. The first vector is unique up to scaling. The second vector can be used to compute a linear combination with the first and can be normalized. This gives the $(s+1)\times(s+1)$ upper triangular parts in $\underline{\mathbf{H}}_9$. The first $s=2$ columns of $\mathbf{U}_9$ and $\underline{\mathbf{H}}_9$ are defined by Arnoldi's method. We remark that some of the leading submatrices of $\mathbf{H}_9$ are singular, e.g., $\mathbf{H}_3$ contains a zero column. It is easy to see that all leading matrices $\mathbf{H}_i$, $i=3,\ldots,9$ are singular by structure.

[1] This is the structure of mneIDR, the structures of srIDR and fmIDR differ from it only in that they have more zeros in the computed $\mathbf{U}_m$. For details we refer to [19].

The eigenvalues of the Sonneveld pencil [13]

$$(\mathbf{H}_m^{\mathrm{S}}, \mathbf{U}_m^{\mathrm{S}}) := (\mathbf{H}_m + \mathbf{U}_m\mathbf{D}_m, \mathbf{U}_m), \tag{2.8}$$

can be used to obtain approximations to the eigenvalues of $\mathbf{A}$. By structure the matrix $\mathbf{H}_m^{\mathrm{S}} - \mu_j\mathbf{U}_m^{\mathrm{S}} = \mathbf{H}_m + \mathbf{U}_m\mathbf{D}_m - \mu_j\mathbf{U}_m$ is singular, i.e., the seed values $\mu_j$, $1 \leqslant j \leqslant k$, are eigenvalues of the Sonneveld pencil. For the sake of clarity we extend example (2.7) and depict the matrix $\mathbf{H}_9^{\mathrm{S}} - \mu_2\mathbf{U}_9^{\mathrm{S}}$:

$$\mathbf{H}_9^{\mathrm{S}} - \mu_2\mathbf{U}_9^{\mathrm{S}} = \mathbf{H}_9 + \mathbf{U}_9(\mathbf{D}_9 - \mu_2\mathbf{I}_9) = \begin{pmatrix} \diamond\circ\bullet\bullet\bullet \\ \circ\diamond\bullet\bullet\bullet \\ \circ\bullet\bullet\bullet \\ \circ\diamond\diamond \\ \circ\diamond \\ \circ \\ \circ\circ\circ\bullet \\ \circ\circ\bullet \\ \circ\bullet \end{pmatrix}. \tag{2.9}$$

The circled elements are the same as in $\mathbf{H}_9$, elements denoted by bullets are elements of $\mathbf{U}_9$ times some difference $\mu_i - \mu_j$, elements denoted by diamonds are combinations of both. The singularity of $\mathbf{H}_m^{\mathrm{S}} - \mu_j\mathbf{U}_m^{\mathrm{S}}$ results from the missing coupling of two consecutive $\mathcal{G}$-spaces.

By defining the *Sonneveld matrix* [13, p. 295] $\mathbf{S}_m := \mathbf{H}_m^{\mathrm{S}}(\mathbf{U}_m^{\mathrm{S}})^{-1}$ we can rewrite the generalized Hessenberg decomposition to return to a Hessenberg decomposition [13, p. 287]. This matrix is a *full* Hessenberg matrix that has the same eigenvalues as the banded Sonneveld pencil, including the seed values $\mu_j$.

**2.3. Purified pencil.** In [13, Lemma 2.1] it was shown that the basis vectors $\mathbf{g}_{k+1}$ can be described in terms of characteristic polynomials of leading sections of the Sonneveld pencil, the matrix $\mathbf{A}$, and the starting vector $\mathbf{g}_1$,

$$\mathbf{g}_{k+1} = g_k(\mathbf{A})\mathbf{g}_1, \quad g_k(z) := \frac{\chi_k(z)}{\prod_{\ell=1}^{k} h_{\ell+1,\ell}}, \quad \chi_k(z) := \mathsf{det}\,(z\mathbf{U}_k^{\mathrm{S}} - \mathbf{H}_k^{\mathrm{S}}). \tag{2.10}$$

This is the IDR-equivalent of the "implicit $\mathbf{Q}$"-Theorem for Arnoldi's method. The polynomials $g_0(z) = 1, g_1, \ldots$ can be computed by *Schweins's recurrence*[2]

$$(g_0, g_1, \ldots, g_{k-1})z\mathbf{U}_k^{\mathrm{S}} = (g_0, g_1, \ldots, g_{k-1}, g_k)\underline{\mathbf{H}}_k^{\mathrm{S}} \tag{2.11}$$

from the Sonneveld pencil and have the root $\mu_j$ once the corresponding block has been reached in the pencil. The polynomials can be purified from the known roots $\mu_j$, the *purified pencil* [13] is obtained from the Sonneveld pencil by omitting multiplication by $z$, this corresponds to altering $\mathbf{U}_m$ by removing the coupling between consecutive $\mathcal{G}$-spaces. The resulting purified $\mathbf{U}_m$ is denoted by $\mathbf{U}_m^{\square}$. The transition is best explained by extending example (2.7); again, $s = 2$ and $m = 9 = 3(s+1)$. $\mathbf{U}_9^{\square}$ is depicted in comparison with $\mathbf{U}_9$,

$$\mathbf{U}_9 = \begin{pmatrix} \circ\bullet\bullet\bullet \\ \circ\bullet\bullet\bullet \\ \circ\bullet\bullet \\ \circ\bullet\bullet\bullet\bullet \\ \circ\bullet\bullet\bullet \\ \circ\bullet\bullet \\ \circ\bullet\bullet \\ \circ\bullet \\ \circ \end{pmatrix}, \quad \mathbf{U}_9^{\square} = \begin{pmatrix} \circ \\ \circ \\ \\ \circ\bullet \\ \circ \\ \\ \\ \circ\bullet \\ \circ \end{pmatrix}. \tag{2.12}$$

Purification is computationally simple, some $(s+1) \times (s+1)$ blocks are blanked out and only unit upper triangular $s \times s$ blocks remain on the diagonal, which are separated by single zero elements on the diagonal. All other entries are unaltered, the *purified pencil* $(\mathbf{H}_m^{\mathrm{S}}, \mathbf{U}_m^{\square})$ with $m = k(s+1)$ has $k$ infinite eigenvalues that replace the seed values, all other eigenvalues are those of the Sonneveld pencil. If some seed value is zero, this process results in a singular pencil; we extend example (2.7) further

[2] We term this recurrence for the recursive computation of scaled determinants of Hessenberg pencils *Schweins's recurrence*, because Schweins [23] was the first to publish a basic form of it [13].

and depict the matrices $\mathbf{H}_9^{\mathrm{s}}$ and $\mathbf{U}_9^{\square}$ for the case $\mu_2 = 0$:

$$\mathbf{H}_9^{\mathrm{s}} = \quad , \qquad \mathbf{U}_9^{\square} = \quad . \tag{2.13}$$

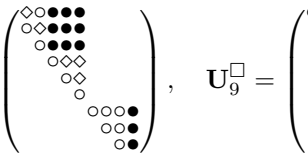

In the inner cycles of IDRStab [25] $\mu = 0$ is used. In [18, pp. 1054–1055] we proved that a regular purified pencil can be obtained by algebraic manipulations that, instead of removing them from the upper triangular $\mathbf{U}_m$, move the negatives of the square blocks from the upper triangular $\mathbf{U}_m$ to the Hessenberg matrix $\mathbf{H}_m^{\mathrm{s}}$. In §4 we show that this is just a special case of a more general approach.

**2.4. Deflated pencil & Lanczos matrix.** It is possible to deflate the pencil to obtain a smaller pencil and get rid of the infinite eigenvalues. A possible deflation is based on block Gaussian elimination, see [13] and [17, §7]. This elimination results in the Schur complement of the submatrix with entries in rows and columns $j(s+1)$, $1 \leqslant j \leqslant k$. This submatrix is the diagonal matrix $\mathsf{diag}(\mu_1, \ldots, \mu_k)$. The purified pencil reordered, such that $\mathsf{diag}(\mu_1, \ldots, \mu_k)$ is the $(1,1)$ block, looks as follows for example (2.7),

$$\mathbf{H}_9^{\mathrm{s}}(\mathsf{index}, \mathsf{index}) = \quad , \qquad \mathbf{U}_9^{\square}(\mathsf{index}, \mathsf{index}) = \quad , \tag{2.14}$$

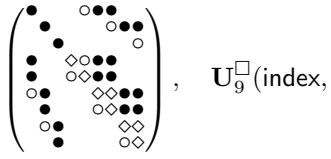

here, $\mathsf{index} = [3, 6, 9, 1, 2, 4, 5, 7, 8]$. Circles in $\mathbf{H}_9^{\mathrm{s}}(\mathsf{index}, \mathsf{index})$ denote elements from $\mathbf{H}_9$, bullets denote elements that are products of elements of $\mathbf{U}_9$ and some $\mu_j$, $1 \leqslant j \leqslant 3$, and diamonds denote sums of both. Circles in $\mathbf{U}_9^{\square}(\mathsf{index}, \mathsf{index})$ denote ones, and the two bullets denote original elements from $\mathbf{U}_9$. Computing the Schur complement

$$\left(\mathbf{H}_{k(s+1)}^{\mathrm{s}} - z\mathbf{U}_{k(s+1)}^{\square}\right) / \mathsf{diag}(\mu_1, \ldots, \mu_k) = \mathbf{H}_{ks}^{\diamond} - z\mathbf{U}_{ks}^{\diamond} \tag{2.15}$$

results in the *deflated pencil* $(\mathbf{H}_{ks}^{\diamond}, \mathbf{U}_{ks}^{\diamond})$, for clarity depicted for our example (2.7) with $k = 3$, $s = 2$:

$$\begin{aligned} \mathbf{H}_6^{\diamond} &= \quad - \quad \quad^{-1} \quad \\ &= \quad , \quad \mathbf{U}_6^{\diamond} = \quad , \end{aligned} \tag{2.16}$$

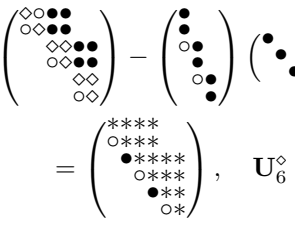

The deflated matrix $\mathbf{H}_{ks}^{\diamond}$ and the Lanczos$(s,1)$ matrix $\mathbf{L}_{ks} := \mathbf{H}_{ks}^{\diamond}(\mathbf{U}_{ks}^{\diamond})^{-1}$ are both upper Hessenberg and block tridiagonal with blocks of size $s \times s$. The circles in $\mathbf{H}_{ks}^{\diamond}$ of example (2.16) denote original nonzero quantities from $\mathbf{H}_{k(s+1)}$ in positions $(\ell + i + 1, \ell + i)$ for $\ell = (j-1)(s+1)$, $1 \leqslant j \leqslant k$, $1 \leqslant i < s$, the bullets are nonzero and given by $-h_{\ell+1,\ell}h_{\ell,\ell-1}/\mu_j$, $\ell = j(s+1)$, $1 \leqslant j < k$. Thus, the matrices $\mathbf{H}_{ks}^{\diamond}$ and $\mathbf{L}_{ks}$ are both *unreduced* upper Hessenberg.

The finite eigenvalues are preserved because of the arising block structure when computing the Schur complement,

$$\det\left(\mathbf{H}_{k(s+1)}^{\mathrm{s}} - z\mathbf{U}_{k(s+1)}^{\square}\right) = \det\left(\mathbf{H}_{ks}^{\diamond} - z\mathbf{U}_{ks}^{\diamond}\right) \cdot \prod_{j=1}^{k} \mu_j. \tag{2.17}$$

Thus, these eigenvalues are also those of the Lanczos$(s,1)$ matrix $\mathbf{L}_{ks} = \mathbf{H}_{ks}^{\diamond}(\mathbf{U}_{ks}^{\diamond})^{-1}$.

**2.5. Finite precision.** In finite precision the basis expansion and the strategy to select the seed values $\mu_j$ become very important. Experiments carried out by the author during the last five years with various different implementations of IDR($s$) showed that basis expansions that use partially orthonormalized vectors are very stable; we will only consider pencils that arise in these. Whereas Lanczos-based methods suffer from multiple copies of Ritz values, Sonneveld methods compute ghost values close to the seed values, which can substantially change the condition of Ritz values nearby. From a computational point of view we are interested in using real arithmetic for real matrices; for real matrices we might want to use solely real seed values. A comparison of the three different basis expansions classified in [18] and various selection schemes for the seed values can be found in the forthcoming report [19]; in [3] selection schemes for the seed values designed for the eigenvalue problem are presented. In this paper we do not consider the choices of the seed values and the IDR variant used; we solely consider the preprocessing part: the stable computation of the eigenvalue approximations defined by the data obtained.

**3. Naive computation of eigenvalues.** We describe very briefly the results of using the mathematical theory sketched in the last section naively to compute the eigenvalues numerically. We collect a few arguments for and against each method. In particular, we are interested in the weaknesses of each approach.

**3.1. Sonneveld matrix & Sonneveld pencil.** Introducing the Sonneveld matrix and thus an ordinary Hessenberg decomposition opens up all possibilities that are known for classical Krylov subspace methods. One immediate disadvantage is that we end up with a *full* Hessenberg matrix, which increases the storage needed. This approach is used in [3] in conjunction with implicit shifts in Francis's (aka the QR) algorithm [11, 12] or implicit filtering [30] in the Hessenberg decomposition. The extended Sonneveld matrix $\underline{\mathbf{S}}_m = \underline{\mathbf{H}}^{\mathrm{S}}_m \mathbf{U}_m^{-1}$ is updated columnwise using the previously computed columns and the last column of $\underline{\mathbf{H}}^{\mathrm{S}}_m$,

$$\underline{\mathbf{S}}_m \mathbf{U}_m = \underline{\mathbf{H}}^{\mathrm{S}}_m, \quad \underline{\mathbf{S}}_m \mathbf{e}_m = \underline{\mathbf{H}}^{\mathrm{S}}_m \mathbf{e}_m - \sum_{\ell<m} \underline{\mathbf{S}}_m \mathbf{e}_\ell u_{\ell,m}. \tag{3.1}$$

The sum is over those few values of $u_{\ell,m}$ that might be nonzero. This is a short recurrence for the computation of the Sonneveld matrix. Close seed values and eigenvalues with large condition numbers might pose a problem, see Figure 3.1. In this

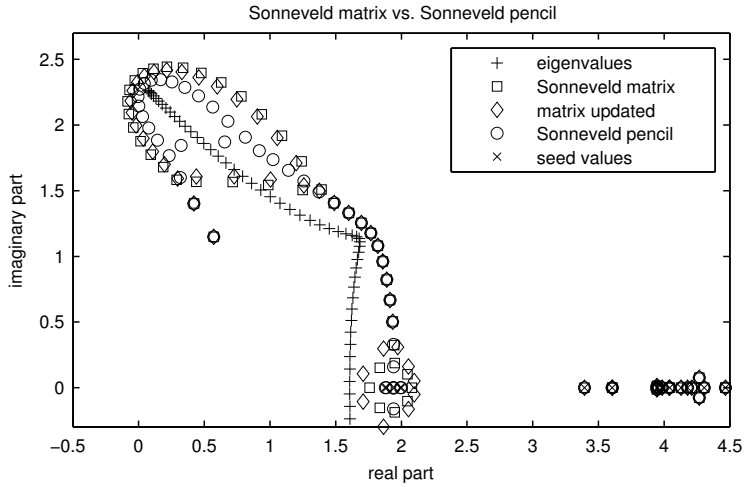


FIG. 3.1. *srIDR*(4) *for* $m = 124$ *steps on a Grcar matrix of size* $n = 100$. *Plus signs depict the computed eigenvalues of* $\mathbf{A}$, *crosses depict the seed values used. Squares depict the computed eigenvalues of the Sonneveld matrix computed by inversion of* $\mathbf{U}_m$, *diamonds depict the computed eigenvalues of the Sonneveld matrix updated via* (3.1), *circles depict the computed eigenvalues of the Sonneveld pencil.*

figure we used srIDR(4), which is the IDR variant used in [34] and [3], on a Grcar matrix of size $n = 100$. This matrix is real, i.e., has complex conjugate eigenvalues. The outer eigenvalues are badly conditioned. The so-called *vanilla strategy* [26] to chose real seed values resulted in some seed values close to the computed Sonneveld Ritz values. For the computation we used MATLAB's `eig` command, i.e., the QR (Francis's) [11, 12] and QZ [16] algorithms. The three different eigenvalue approximations coincide in theory; the difference is due to the conditioning of the different representations. The best results are obtained by using the Sonneveld pencil.

As to be expected [16, p. 254], QZ beats QR: QZ on the Sonneveld pencil with explicit deflation of seed values, similar to [3], behaves better than QR on the Sonneveld matrix. The drawback is that the unitary deflation or any other steps of QZ result in a *full* Hessenberg/upper triangular pencil. In standard software no deflation of seed values is possible, we have to alter parts of the code or to write some preprocessing routine. A variant of the LZ algorithm [15] with restricted pivoting preserves the structure at the expense of increasing the conditioning of the eigenvalues.

Even for the Sonneveld pencil, close seed values might be harmful, even when we deflate first, which can be seen on the real axis in Figure 3.1: close to a genuine eigenvalue approximation on the real axis there are several approximations that correspond to seed values. It is hard to distinguish seed values and eigenvalue approximations, especially, as Ritz values close to seed values may be ghost values, visible close to the real axis in the interval $[3, 5]$.

**3.2. Purified pencil.** We use the data computed for Figure 3.1 and invoke QZ on the purified pencil. The resulting Figure 3.2 shows that this gives only one eigenvalue approximation in the real cluster near 2 and gives even better approximations of the badly conditioned eigenvalues. This need not be the case, as counterexample consider

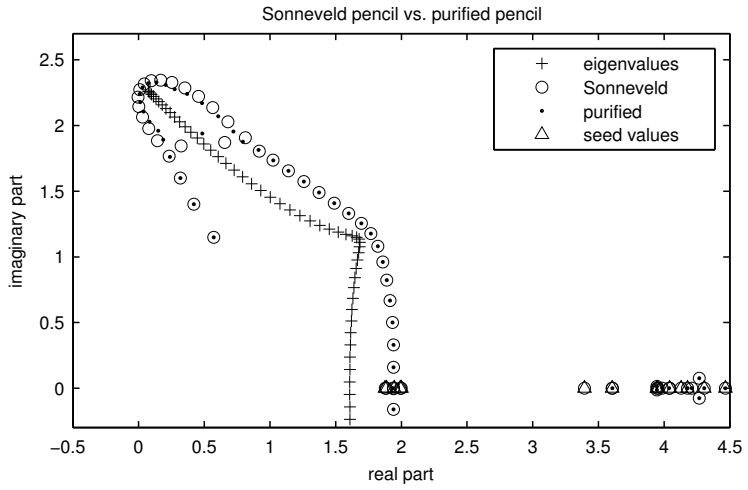


FIG. 3.2. *srIDR(4) for $m = 124$ steps on a Grcar matrix of size $n = 100$, vanilla strategy. Plus signs depict computed eigenvalues, triangles the seed values. Circles depict computed eigenvalues of the Sonneveld pencil, dots depict computed eigenvalues of the purified pencil.*

Figure 3.3. In this example we used the same shadow vectors and starting vector as in the previous example, only the strategy to select the seed values was changed. The seed value selection scheme gives many small seed values. In this case we observe a drastical difference between the approximations obtained using the Sonneveld and the purified pencil. The reason is that the purified pencil is badly conditioned due to the small seed values that give an almost singular pencil.

Thus, if we want to use the purified pencil from §2.3, we either have to use a technique that ensures a good condition, or we can use special QZ-like algorithms. A good condition is typically obtained, if we are close to the Lanczos$(s, 1)$ data, which is

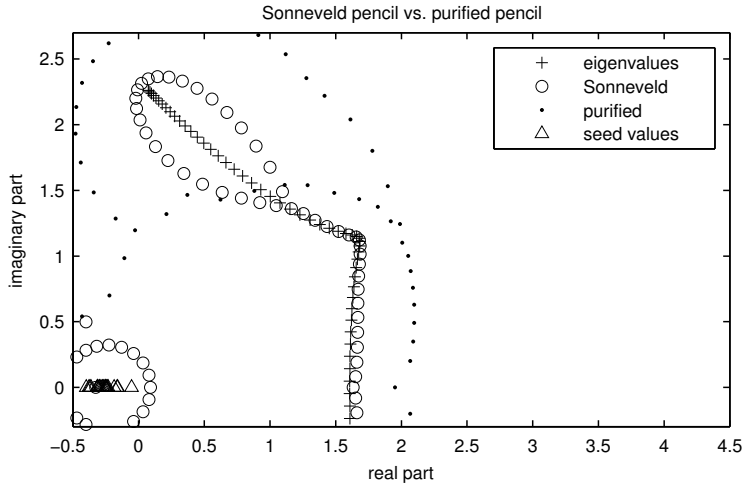


FIG. 3.3. *srIDR*(4) *for* $m = 124$ *steps on a Grcar matrix of size* $n = 100$*, different seed value selection scheme. Plus signs depict computed eigenvalues, triangles the seed values. Circles depict computed eigenvalues of the Sonneveld pencil, dots depict computed eigenvalues of the purified pencil.*

the case, e.g., for the vanilla selection scheme. If $\mu = 0$, we can use a method designed for singular pencils, possibly with known ranks, e.g., GUPTRI [5, 6] or other staircase algorithms.

For Hermitian ill-conditioned pencils methods do exist that extract eigenvalues, see [10]. In contrast, no stable method exists for almost singular pencils as the one corresponding to Figure 3.3. We remark that the seed value selection scheme used in this example is superior to the vanilla strategy for all eigenvalues with real part greater or equal one. One way is to discard the purified pencil and stick to the Sonneveld pencil, another way is presented in §6, where we show that we can compute the eigenvalue approximations with an alternate purified pencil. In any case, if we use a standard QZ algorithm on the purified pencil, we destroy the structure and obtain a full upper Hessenberg/upper triangular pencil.

**3.3. Deflated pencil & Lanczos matrix.** The deflated pencil might not exist due to zero seed values or be badly conditioned due to small seed values, as we compute the Schur complement of the diagonal matrix $\mathsf{diag}(\mu_1, \ldots, \mu_k)$. If we use the QZ algorithm, we end up with a full upper Hessenberg/upper triangular pencil. Using the LZ algorithm [15] 'as is' does not help, again we obtain a full upper Hessenberg/upper triangular pencil. Like for the Sonneveld pencil, the structure is preserved if we restrict the permutations to respect the structure, thus potentially increasing the instabilities of LZ.

Explicitely computing the Lanczos matrix will typically result in a worse conditioning of its eigenvalues. Using Francis's QR algorithm on the Lanczos matrix will result in a full Hessenberg matrix. If we use Rutishauser's LR algorithm [21, 22] on the Lanczos matrix without pivoting across blocks, we preserve the band structure. Unfortunately, the approach to compute the Ritz values using the Lanczos$(s, 1)$ matrix is mostly very badly conditioned. If it were not, we could use the LR algorithm with some sort of threshold pivoting to only slightly increase the bandwith. In case of real matrices we would like to use the implicit double-shift LR [37, p. 537].

Suppose that we could obtain the Lanczos matrix in a stable way. We would like to use a variant of qd [20] on the Lanczos matrix, preferably something similar to dqds [7]. For $s = 1$ we could use complex dqds or tridqds [8, 9]. For $s > 1$ there do exist some block generalizations of qd, namely block QD by [38], a block qds for arbitrary quasiseparable matrices and a dqds for Hessenberg $(1, s)$-quasiseparable matrices [41]. In contrast to the dqds for Hessenberg $(1, 1)$-quasiseparable nonnegative matrices in

[4], the latter comes with no proof for stability, but is the only algorithm of dqds type the author is aware of that could be applied to the Lanczos matrix.

**4. Families of pencils with identical eigenvalues.** In this section we prove that Sonneveld methods compute one-dimensional families of pencils that have the same eigenvalues. The proof is based on the translation invariance of the structure.

**4.1. A purified family.** The data that defines the Sonneveld pencil defines infinitely many purified pencils, the purified pencil presented in §2 corresponds to the instance $\tau = 0$ in the following theorem.

THEOREM 4.1. *Suppose that* $\mathbf{H}_m$, $\mathbf{U}_m$, $m = k(s+1)$ *and* $\mu_j$, $1 \leqslant j \leqslant k$ *define a Sonneveld pencil* (2.8) *with eigenvalues* $\mu_1, \ldots, \mu_k$ *and* $\theta_i$, $1 \leqslant i \leqslant ks$. *Let* $\mathbf{U}_m^{\square}$ *denote* $\mathbf{U}_m$ *after purification, and define the matrix of removed blocks by* $\mathbf{U}_m^{\blacksquare} := \mathbf{U}_m - \mathbf{U}_m^{\square}$. *Then every member of the family*

$$(\mathbf{H}_m^{\mathrm{s}} - \tau \mathbf{U}_m^{\blacksquare}, \mathbf{U}_m^{\square}), \quad \tau \in \mathbb{C} \setminus \{\mu_1, \ldots, \mu_k\} \tag{4.1}$$

*of pencils has* $k$ *infinite eigenvalues and the eigenvalues* $\theta_i$, $1 \leqslant i \leqslant ks$.

*Proof.* The shifted pencil $(\mathbf{H}_m^{\mathrm{s}} - \tau \mathbf{U}_m, \mathbf{U}_m)$ has the eigenvalues $\mu_1 - \tau, \ldots, \mu_k - \tau$ and $\theta_i - \tau$, $1 \leqslant i \leqslant ks$. The block structure is preserved: purification of the characteristic polynomials from the known nonzero roots $\mu_1 - \tau, \ldots, \mu_k - \tau$ works exactly in the same manner as sketched in §2.3. The pencil $(\mathbf{H}_m^{\mathrm{s}} - \tau \mathbf{U}_m, \mathbf{U}_m^{\square})$ has $k$ infinite eigenvalues and the eigenvalues $\theta_i - \tau$, $1 \leqslant i \leqslant ks$. We shift back by $\tau$ and obtain the pencil $(\mathbf{H}_m^{\mathrm{s}} - \tau \mathbf{U}_m + \tau \mathbf{U}_m^{\square}, \mathbf{U}_m^{\square})$ that has $k$ infinite eigenvalues and the eigenvalues $\theta_i$, $1 \leqslant i \leqslant ks$. ∎

The pencils obtained for $\tau = \mu_j$, $j = 1, \ldots, k$ are singular, the example $\tau = \mu_2$, $s = 2$, $m = 9 = 3(s+1)$ looks structurally identical to example (2.13). Without realizing it at that time, we used $\tau = 1$ in our derivation [18, pp. 1051–1055] of a purified pencil in case of IDRStab [25].

The eigenvalues are shift-invariant; the eigenvectors are not. This is obvious, as the pencils change with respect to the parameter $\tau$; the impact of this change on the eigenvectors is clarified in the next theorem.

THEOREM 4.2. *Let the notation be as in Theorem 4.1. Define the bivariate eigenvector polynomials* $\check{\boldsymbol{\nu}}(z, \tau) \in \mathbb{C}^m[z, \tau]$ *and* $\boldsymbol{\nu}(z, \tau) \in \mathbb{C}^m[z, \tau]$ *by*

$$\check{\boldsymbol{\nu}}(z, \tau) := \big(\check{\nu}_1(z, \tau), \ldots, \check{\nu}_m(z, \tau)\big)^{\mathsf{T}}, \quad \boldsymbol{\nu}(z, \tau) := \big(\nu_1(z, \tau), \ldots, \nu_m(z, \tau)\big)^{\mathsf{T}}, \tag{4.2}$$

*where*

$$\begin{aligned} \check{\nu}_i(z, \tau) &:= \frac{\det\left(z\mathbf{U}_{1:i-1}^{\square} + \tau \mathbf{U}_{1:i-1}^{\blacksquare} - \mathbf{H}_{1:i-1}^{\mathrm{s}}\right)}{\prod_{\ell=1}^{i-1} h_{\ell+1,\ell}}, \\ \nu_i(z, \tau) &:= \frac{\det\left(z\mathbf{U}_{i+1:m}^{\square} + \tau \mathbf{U}_{i+1:m}^{\blacksquare} - \mathbf{H}_{i+1:m}^{\mathrm{s}}\right)}{\prod_{\ell=i+1}^{m} h_{\ell,\ell-1}}, \end{aligned} \qquad 1 \leqslant i \leqslant m, \tag{4.3}$$

*with the convention that* $\check{\nu}_1(z, \tau) = \nu_m(z, \tau) = 1$. *Then, for all* $\tau \in \mathbb{C}$, $1 \leqslant i \leqslant ks$,

$$\begin{aligned} \check{\boldsymbol{\nu}}(\theta_i, \tau)^{\mathsf{T}}(\mathbf{H}_m^{\mathrm{s}} - \tau \mathbf{U}_m^{\blacksquare}) &= \check{\boldsymbol{\nu}}(\theta_i, \tau)^{\mathsf{T}} \theta_i \mathbf{U}_m^{\square}, \\ (\mathbf{H}_m^{\mathrm{s}} - \tau \mathbf{U}_m^{\blacksquare})\boldsymbol{\nu}(\theta_i, \tau) &= \theta_i \mathbf{U}_m^{\square} \boldsymbol{\nu}(\theta_i, \tau). \end{aligned} \tag{4.4}$$

*The eigenvector polynomials factor componentwise, i.e., with* $M_{i:j}(\tau) := \prod_{\ell=i}^{j}(\tau - \mu_\ell)$,

$$
\begin{aligned}
\check{\boldsymbol{\nu}}(z,\tau) = \Big(&\check{\rho}_1(z), \check{\rho}_2(z), \ldots, \check{\rho}_s(z), \check{\varrho}_{s+1}(z),\\
&(\tau-\mu_1)\check{\rho}_{s+1}(z), (\tau-\mu_1)\check{\rho}_{s+2}(z), \ldots,\\
&\quad (\tau-\mu_1)\check{\rho}_{2s}(z), (\tau-\mu_1)\check{\varrho}_{2s+1}(z),\\
&(\tau-\mu_1)(\tau-\mu_2)\check{\rho}_{2s+1}(z), (\tau-\mu_1)(\tau-\mu_2)\check{\rho}_{2s+2}(z), \ldots,\\
&\quad (\tau-\mu_1)(\tau-\mu_2)\check{\rho}_{3s}(z), (\tau-\mu_1)(\tau-\mu_2)\check{\varrho}_{3s+1}(z), \ldots,\\
&M_{k-1}(\tau)\check{\rho}_{(k-1)s+1}(z), M_{k-1}(\tau)\check{\rho}_{(k-1)s+2}(z), \ldots,\\
&\qquad M_{k-1}(\tau)\check{\rho}_{ks}(z), M_{k-1}(\tau)\check{\varrho}_{ks+1}(z)\Big)^{\mathsf{T}},
\end{aligned}
\tag{4.5a}
$$

$$
\begin{aligned}
\boldsymbol{\nu}(z,\tau) = \Big(&M_{1:k}(\tau)\rho_1(z), M_{1:k}(\tau)\rho_2(z), \ldots, M_{1:k}(\tau)\rho_s(z),\\
&\quad M_{2:k}(\tau)\varrho_s(z),\\
&M_{2:k}(\tau)\rho_{s+1}(z), M_{2:k}(\tau)\rho_{s+2}(z), \ldots, M_{2:k}(\tau)\rho_{2s}(z),\\
&\quad M_{3:k}(\tau)\varrho_{2s}(z), \ldots,\\
&M_{k-1:k}(\tau)\rho_{(k-2)s+1}(z), M_{k-1:k}(\tau)\rho_{(k-2)s+2}(z), \ldots, M_{k-1:k}(\tau)\rho_{(k-1)s}(z),\\
&\quad (\tau-\mu_k)\varrho_{(k-1)s}(z),\\
&(\tau-\mu_k)\rho_{(k-1)s+1}(z), (\tau-\mu_k)\rho_{(k-1)s+2}(z), \ldots,\\
&\qquad (\tau-\mu_k)\rho_{ks}(z), \varrho_{ks}(z)\Big)^{\mathsf{T}}.
\end{aligned}
\tag{4.5b}
$$

*Proof.* We know from [13, Lemma 2.1], a result already anticipated in [39, §5], that

$$
\begin{aligned}
\check{\boldsymbol{\nu}}(z,\tau)^{\mathsf{T}}(z\mathbf{U}_m^{\square} + \tau\mathbf{U}_m^{\blacksquare} - \mathbf{H}_m^{\mathrm{s}}) &= \frac{\chi(z,\tau)}{\prod_{\ell=1}^{m-1} h_{\ell+1,\ell}}\mathbf{e}_m^{\mathsf{T}},\\
(z\mathbf{U}_m^{\square} + \tau\mathbf{U}_m^{\blacksquare} - \mathbf{H}_m^{\mathrm{s}})\boldsymbol{\nu}(z,\tau) &= \mathbf{e}_1\frac{\chi(z,\tau)}{\prod_{\ell=1}^{m-1} h_{\ell+1,\ell}},
\end{aligned}
\tag{4.6}
$$

where $\chi(z,\tau) := \mathsf{det}\,(z\mathbf{U}_m^{\square} + \tau\mathbf{U}_m^{\blacksquare} - \mathbf{H}_m^{\mathrm{s}})$, which has the roots $z = \theta_i$ for all $\tau$. Thus, the eigenvector polynomials evaluated at $z = \theta_i$ give the corresponding eigenvectors. Not only the characteristic polynomial factors into a product of a univariate polynomial in $z$ and a univariate polynomial in $\tau$, all trailing and leading characteristic polynomials factor in a similar manner. We only give the proof for the left eigenvector polynomial coefficients, the proof for the right eigenvector polynomial coefficients is analogous. It helps to keep in mind that $\mathbf{U}_m^{\blacksquare}$ contains the interactions between consecutive blocks. The first $s$ columns of $\mathbf{U}_m^{\blacksquare}$ are zero, thus, the degree of $\check{\nu}_j(z,\tau)$ as polynomial in $\tau$ is zero for $j = 1, \ldots, s+1$. The next $s+1$ columns are zero below the $s+1$st row, the element in position $(s+1, s+1)$ is given by $\tau$. This implies that the degree of $\check{\nu}_j(z,\tau)$ as polynomial in $\tau$ is one for $s+2 \leqslant j \leqslant 2s+2$. This pattern repeats itself, the degree as polynomial in $\tau$ increases by one after every multiple of $s+1$. Setting $\tau = \mu_j$, $1 \leqslant j \leqslant k$, results in a right upper zero block that has its lower left corner on the diagonal, i.e., every characteristic polynomial of a pencil that contains such a diagonal element has a linear factor $\tau - \mu_j$, where $\mu_j$ is the seed value of the corresponding block. Dividing by the known linear factors we end up with a left set of polynomials $\{\check{\rho}_\ell\}$ and (some members of) a second left set of polynomials $\{\check{\varrho}_\ell\}$, its elements in both cases univariate in $z$ of degree $\ell - 1$. The corresponding elements of the right sets of polynomials $\{\rho_\ell\}$ and (for some $\ell$) $\{\varrho_\ell\}$ have degree $ks - \ell$; by construction, $\check{\rho}_1(z) = \varrho_{ks+1}(z) = 1$. □

We remark that the computation of $\mathbf{U}_m^{\square}$ and $\mathbf{U}_m^{\blacksquare}$ from $\mathbf{U}_m$ is exact, even in finite precision. We have a family of pencils at hand to compute the wanted eigenvalues, the only difference is in the corresponding eigenvectors and thus the eigenvalue condition numbers. For $\tau = \mu_i$ the resulting pencil is singular; the shift should be far from the seed values, but not to close to infinity.

We computed a Sonneveld pencil using mnelDR(3) for $m = 39$ steps on a Grcar matrix of size $n = 30$ and plotted the normwise condition numbers of the simple, finite,

nonzero eigenvalues $\theta_i$ [14, eq. (2.9), Theorem 2.5] of the family of purified pencils (4.1) for the Euclidean norm and absolute errors,

$$\kappa(\theta_i,\tau) := \limsup_{\epsilon\to 0}\Big\{ \frac{|\Delta\theta_i|}{\epsilon|\theta_i|} \mid (\mathbf{H}_m^{\mathrm{S}} - \tau\mathbf{U}_m^{\blacksquare} + \Delta\mathbf{H}_m)(\boldsymbol{\nu}(\theta_i,\tau)+\Delta\boldsymbol{\nu}) = (\theta_i+\Delta\theta_i)(\mathbf{U}_m^{\square}+\Delta\mathbf{U}_m)(\boldsymbol{\nu}(\theta_i,\tau)+\Delta\boldsymbol{\nu}) \quad (4.7)$$
$$\|\Delta\mathbf{H}_m\| \leqslant \epsilon\|\mathbf{H}_m^{\mathrm{S}} - \tau\mathbf{U}_m^{\blacksquare}\|, \quad \|\Delta\mathbf{U}_m\| \leqslant \epsilon\|\mathbf{U}_m^{\square}\| \Big\}$$
$$= \frac{\|\check{\boldsymbol{\nu}}(\theta_i,\tau)\|\|\boldsymbol{\nu}(\theta_i,\tau)\|(\|\mathbf{H}_m^{\mathrm{S}} - \tau\mathbf{U}_m^{\blacksquare}\| + |\theta_i|\|\mathbf{U}_m^{\square}\|)}{|\theta_i||\check{\boldsymbol{\nu}}(\theta_i,\tau)^{\mathsf{T}}\mathbf{U}^{\square}\boldsymbol{\nu}(\theta_i,\tau)|}. \quad (4.8)$$

We used MATLAB's symbolic math toolbox, i.e., the MuPAD kernel, to compute the exact bivariate eigenvector polynomials, substituted the numerically computed eigenvalues of the purified pencil for $\tau = 1$ and numerically computed the norms of the matrices involved. The resulting Figure 4.1 shows the expected behaviour. The

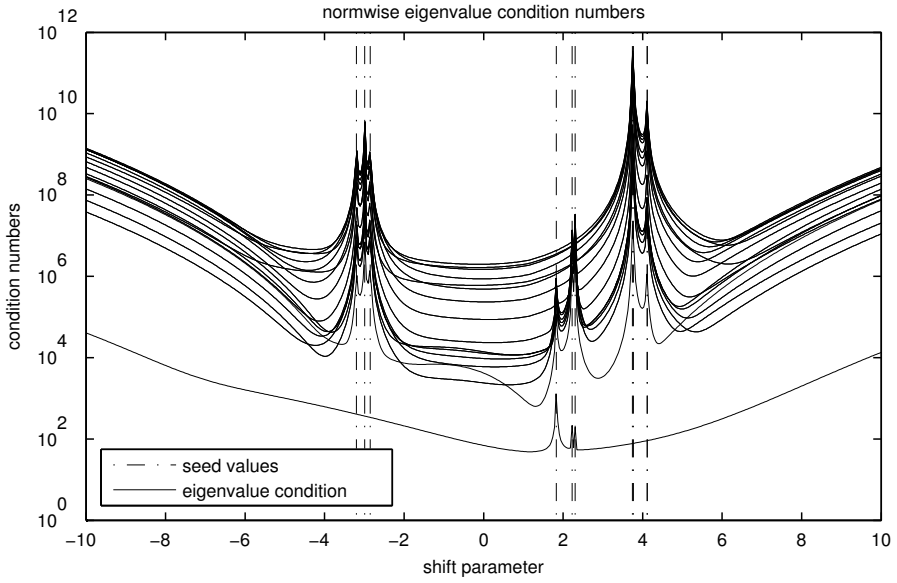


FIG. 4.1. *Normwise condition numbers of all* 30 *eigenvalues of the family of purified pencils computed by* mneIDR(3) *for* $m = 39$ *steps on a Grcar matrix of size* $n = 30$ *with the vanilla seed value selection scheme.*

two lowest condition number curves correspond to the real Ritz values close to one and close to four, clearly visible in Figure 4.2. In this figure we depict the computed eigenvalue approximations. The condition numbers close to the seed values are very large. This is even more pronounced if two or more seed values coalesce, which is almost the case in our example, where $\mu_2 \approx 3.7400$ and $\mu_3 \approx 3.7691$. We also observe the expected increase in the condition numbers for $\tau$ far from the spectrum and the seed values.

As the normwise condition numbers do not respect the structure, which is done in part even by QZ, more by LZ, we depict the componentwise condition number of the

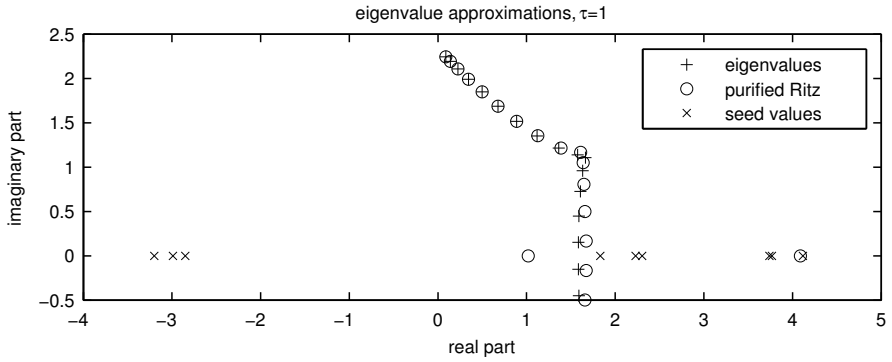


FIG. 4.2. *Eigenvalue approximations by the* 30 *Ritz values computed by* mnelDR(3) *for* $m = 39$ *steps on a Grcar matrix of size* $n = 30$ *with the vanilla seed value selection scheme.*

simple, finite, nonzero eigenvalues $\theta_i$ [14, eq. (3.4), Theorem 3.2]

$$\begin{aligned}\mathsf{cond}(\theta_i,\tau) := \limsup_{\epsilon\to 0}\Big\{ \frac{|\Delta\theta_i|}{\epsilon|\theta_i|} \mid (\mathbf{H}_m^{\mathrm{S}} - \tau\mathbf{U}_m^{\blacksquare} + \Delta\mathbf{H}_m)(\boldsymbol{\nu}(\theta_i,\tau) + \Delta\boldsymbol{\nu}) = \\ (\theta_i + \Delta\theta_i)(\mathbf{U}_m^{\square} + \Delta\mathbf{U}_m)(\boldsymbol{\nu}(\theta_i,\tau) + \Delta\boldsymbol{\nu}) \qquad (4.9)\\ |\Delta\mathbf{H}_m| \leqslant \epsilon|\mathbf{H}_m^{\mathrm{S}} - \tau\mathbf{U}_m^{\blacksquare}|, \quad |\Delta\mathbf{U}_m| \leqslant \epsilon|\mathbf{U}_m^{\square}| \Big\}\end{aligned}$$

$$= \frac{|\check{\boldsymbol{\nu}}(\theta_i,\tau)^{\mathsf{T}}||\mathbf{H}_m^{\mathrm{S}} - \tau\mathbf{U}_m^{\blacksquare}||\boldsymbol{\nu}(\theta_i,\tau)| + |\theta_i||\check{\boldsymbol{\nu}}(\theta_i,\tau)^{\mathsf{T}}||\mathbf{U}_m^{\square}||\boldsymbol{\nu}(\theta_i,\tau)|}{|\theta_i||\check{\boldsymbol{\nu}}(\theta_i,\tau)^{\mathsf{T}}\mathbf{U}^{\square}\boldsymbol{\nu}(\theta_i,\tau)|} \qquad (4.10)$$

in Figure 4.3. It is clearly visible that the componentwise eigenvalue condition is

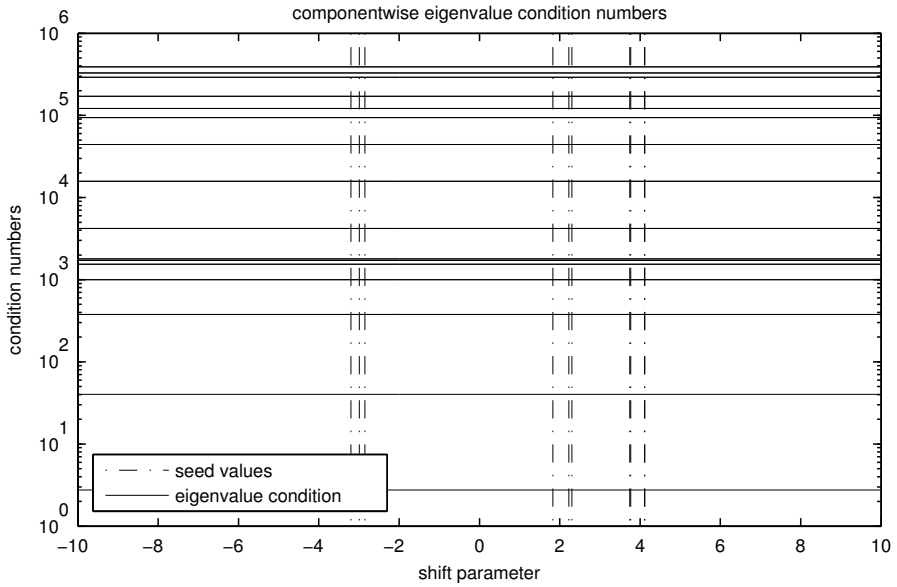


FIG. 4.3. *Componentwise condition numbers of all* 30 *eigenvalues of the family of purified pencils computed by* mnelDR(3) *for* $m = 39$ *steps on a Grcar matrix of size* $n = 30$ *with the vanilla seed value selection scheme.*

independent of the shift[3], which follows from the block structure of the matrices, the factorization of the bivariate eigenvector polynomials (4.5), and the formula (4.10) for

[3]We computed the data for this plot using MATLAB's symbolic math toolbox, unaware of this fact. The computation of these few horizontal lines took two days.

the componentwise condition numbers. The componentwise condition numbers are smaller than the best corresponding normwise condition numbers, but still larger than the corresponding Wilkinson's eigenvalue condition numbers of the eigenvalues of the Grcar matrix that are approximated by them.

There does not exist a solver for these structured pencils that will not destroy the structure. The observed behaviour lies somewhere between both, the normwise, and the componentwise world. As a rule of thumb: the more structure is preserved, the better the structured eigenvalue condition numbers.

**4.2. A deflated family.** The computation of the Schur complements of the purified pencils results in a family of deflated pencils. This family turns out to be just a structured block-diagonal scaling of a single pencil.

THEOREM 4.3. *Let the notation be as in Theorem 4.1. The family of deflated pencils obtained by computation of the Schur complement is given by*

$$(\mathbf{H}^{\diamond}_{ks}(\tau), \mathbf{U}^{\diamond}_{ks}), \quad \mathbf{H}^{\diamond}_{ks}(\tau), \mathbf{U}^{\diamond}_{ks} \in \mathbb{C}^{ks\times ks}, \quad \tau \in \mathbb{C} \setminus \{\mu_1, \ldots, \mu_k\}, \tag{4.11}$$

*where* $\mathbf{H}^{\diamond}_{ks} = \mathbf{H}^{\diamond}_{ks}(0)$*, and the unreduced Hessenberg block tridiagonal matrices* $\mathbf{H}^{\diamond}_{ks}(\tau)$*,* $\tau \in \mathbb{C} \setminus \{\mu_1, \ldots, \mu_k\}$*, are defined as*

$$\mathbf{H}^{\diamond}_{ks}(\tau) := \begin{pmatrix} \mathbf{h}^{\bullet}_{1,1} & (\tau-\mu_1)\mathbf{h}^{\bullet}_{1,2} & & \\ \dfrac{\mathbf{h}^{\bullet}_{2,1}}{\tau-\mu_1} & \mathbf{h}^{\bullet}_{2,2} & \ddots & \\ & \ddots & \ddots & (\tau-\mu_{k-1})\mathbf{h}^{\bullet}_{k-1,k} \\ & & \dfrac{\mathbf{h}^{\bullet}_{k,k-1}}{\tau-\mu_{k-1}} & \mathbf{h}^{\bullet}_{k,k} \end{pmatrix}, \tag{4.12}$$

*with the non-trivial blocks* $\mathbf{h}^{\bullet}_{i,j} \in \mathbb{C}^{s\times s}$*,* $1 \leqslant i, j \leqslant k$*,* $|i-j| \leqslant 1$*, given by*

$$\begin{aligned}
\mathbf{h}^{\bullet}_{1,1} &:= \mathbf{H}_{1:s,1:s} - \mathbf{U}_{1:s,s+1} h_{s+1,s} \mathbf{e}_s^{\mathsf{T}}, && (4.13a)\\
\mathbf{h}^{\bullet}_{i,i} &:= \mathbf{H}_{i(s+1)-s:i(s+1)-1,i(s+1)-s:i(s+1)-1} \\
&\quad + \mu_{i-1}\mathbf{U}_{i(s+1)-s:i(s+1)-1,i(s+1)-s:i(s+1)-1}, \quad 2 \leqslant i \leqslant k, && (4.13b)\\
\mathbf{h}^{\bullet}_{i+1,i} &:= h_{i(s+1)+1,i(s+1)} h_{i(s+1),i(s+1)-1} \mathbf{e}_1 \mathbf{e}_s^{\mathsf{T}}, \quad 1 \leqslant i < k, && (4.13c)\\
\mathbf{h}^{\bullet}_{i,i+1} &:= \mathbf{U}_{i(s+1)-s:i(s+1)-1,i(s+1)} \mathbf{U}_{i(s+1),i(s+1)+1:i(s+1)+s} \\
&\quad - \mathbf{U}_{i(s+1)-s:i(s+1)-1,i(s+1)+1:i(s+1)+s} \\
&\quad - \mathbf{U}_{(i+1)(s+1)-s:(i+1)(s+1)-1,(i+1)(s+1)} h_{(i+1)(s+1),(i+1)(s+1)-1} \mathbf{e}_s^{\mathsf{T}} \\
&\quad - \mathbf{e}_1 h_{i(s+1)+1,i(s+1)} \mathbf{U}_{i(s+1),i(s+1)+1:i(s+1)+s}, \quad 1 \leqslant i < k. && (4.13d)
\end{aligned}$$

*All members of the family of deflated pencils (4.11) are block diagonally similar to the* basic deflated pencil $(\mathbf{H}^{\bullet}_{ks}, \mathbf{U}^{\bullet}_{ks})$*, where*

$$\mathbf{H}^{\bullet}_{ks} := \begin{pmatrix} \mathbf{h}^{\bullet}_{1,1} & \mathbf{h}^{\bullet}_{1,2} & & \\ \mathbf{h}^{\bullet}_{2,1} & \mathbf{h}^{\bullet}_{2,2} & \ddots & \\ & \ddots & \ddots & \mathbf{h}^{\bullet}_{k-1,k} \\ & & \mathbf{h}^{\bullet}_{k,k-1} & \mathbf{h}^{\bullet}_{k,k} \end{pmatrix}, \quad \mathbf{U}^{\bullet}_{ks} := \mathbf{U}^{\diamond}_{ks}. \tag{4.14}$$

*The basic deflated pencil has the left and right eigenvectors* $\check{\boldsymbol{\rho}}(\theta_j)$ *and* $\boldsymbol{\rho}(\theta_j)$*, where*

$$\check{\boldsymbol{\rho}}(z) := \Big(\check{\rho}_1(z), \ldots, \check{\rho}_{ks}(z)\Big)^{\mathsf{T}}, \quad \boldsymbol{\rho}(z) := \Big(\rho_1(z), \ldots, \rho_{ks}(z)\Big)^{\mathsf{T}}, \tag{4.15}$$

*with* $\check{\rho}_\ell(z)$ *and* $\rho_\ell(z)$*,* $1 \leqslant \ell \leqslant ks$*, defined in (4.5).*

*Proof.* The Schur complement is computed following the steps outlined in section 2.4. Careful examination of the structure depicted in example (2.16) shows that

some terms $\tau - \mu_j$ cancel and that the matrix (4.12) with the elements (4.13) arises. Let $\mathbf{I} \in \mathbb{C}^{s\times s}$. The diagonal similarity transformation $\mathbf{T}(\tau)$,

$$\mathbf{T}(\tau)(\mathbf{H}^{\diamond}_{ks}(\tau), \mathbf{U}^{\diamond}_{ks})(\mathbf{T}(\tau))^{-1} = (\mathbf{H}^{\bullet}_{ks}, \mathbf{U}^{\bullet}_{ks}), \tag{4.16}$$

of the family (4.11) of pencils to the basic deflated pencil (4.14) is given by

$$\mathbf{T}(\tau) := \mathsf{diag}(\mathbf{I}, M_1(\tau)\mathbf{I}, M_2(\tau), \ldots, M_{k-1}(\tau)). \tag{4.17}$$

The Schur complement is connected to left and right block Gaussian elimination. To understand the impact of deflation on the right eigenvectors, we look at the right block Gaussian eliminator $\mathbf{M}_m$ [13, Eqn. (4.33)], which, when applied from the right, transforms the family (4.1) of purified pencils to the pencils

$$(\mathbf{H}^{\mathrm{s}}_m - \tau\mathbf{U}^{\blacksquare}_m, \mathbf{U}^{\square}_m)\mathbf{M}_m = (\widetilde{\mathbf{H}}_m(\tau), \mathbf{U}^{\square}_m), \quad \widetilde{\mathbf{H}}_m(\tau) := \begin{pmatrix} \bullet\bullet\circ\bullet\bullet & & & \\ \bullet\bullet\circ\bullet\bullet & & & \\ & \circ & & \\ & \bullet\circ\bullet\bullet\circ\bullet\bullet & & \\ & & \bullet\bullet\circ\bullet\bullet & \\ & & & \circ \\ & & & \bullet\circ\bullet\bullet\circ \\ & & & & \bullet\bullet\circ \\ & & & & & \circ \end{pmatrix}, \tag{4.18}$$

where the bullets denote the elements of $\mathbf{H}^{\diamond}_{ks}(\tau)$, and the circles denote original elements, here depicted for $s = 2$, $m = k(s+1) = 9$. The matrix $\mathbf{M}_m$ looks structurally as follows for the example $s = 2$, $m = k(s+1) = 9$ of the purified pencil (2.12):

$$\mathbf{M}_9 := \begin{pmatrix} \circ & & & & & & & & \\ & \circ & & & & & & & \\ & \bullet\circ\bullet\bullet & & & & & & & \\ & & \circ & & & & & & \\ & & & \circ & & & & & \\ & & & \bullet\circ\bullet\bullet & & & & & \\ & & & & \circ & & & & \\ & & & & & \circ & & & \\ & & & & & \bullet\circ & & & \end{pmatrix}, \quad \begin{pmatrix} \circ & & & & & & & & \\ & \circ & & & & & & & \\ & \bullet\circ\bullet\bullet & & & & & & & \\ & & \circ & & & & & & \\ & & & \circ & & & & & \\ & & & \bullet\circ\bullet\bullet & & & & & \\ & & & & \circ & & & & \\ & & & & & \circ & & & \\ & & & & & \bullet\circ & & & \end{pmatrix}^{-1} = \begin{pmatrix} \circ & & & & & & & & \\ & \circ & & & & & & & \\ & *\circ** & & & & & & & \\ & & \circ & & & & & & \\ & & & \circ & & & & & \\ & & & *\circ** & & & & & \\ & & & & \circ & & & & \\ & & & & & \circ & & & \\ & & & & & *\circ & & & \end{pmatrix} = \mathbf{M}_9^{-1}. \tag{4.19}$$

Here, the circles in the diagonal denote ones, and the stars in the right-hand side are the negatives of the bullets in the left-hand side in the same position. As the eigenvectors of the pencils on the right-hand side of (4.18) are given by $\mathbf{M}_m^{-1}$ times those of the purified pencils, which are given by (4.5), and because $\mathbf{M}_m^{-1}$ modifies only every entry with index $j(s+1)$, $1 \leqslant j \leqslant k$, all other eigenvector entries remain unchanged. Deflation can be described as omitting exactly the indices that correspond to those that have been changed. Thus, the right eigenvectors of the deflated pencils (4.11) consist of the right eigenvectors of the purified pencils (4.5), omitting every entry with index $j(s+1)$, $1 \leqslant j \leqslant k$. The scaling that results in the basic deflated pencil causes the common factor $M_k(\tau)$ in all entries, which is left out for simplicity. The last element $\rho_{ks}(z)$ is constant; by definition of $\mathbf{U}_m$, the diagonal element $u_{m,m}$ is one, and by definition of the bivariate eigenvector polynomials (4.3),

$$\nu_{m-1}(z,\tau) = \frac{(\tau - \mu_k)u_{m,m}}{h_{m,m-1}}, \quad \text{i.e.,} \quad \rho_{ks}(z) = h^{-1}_{m,m-1} \neq 0.$$

This proves that the right polynomial vector in (4.15) defines the right eigenvectors of the basic deflated pencil. A similar derivation proves that the inverse of the left block Gaussian eliminator, when applied from the right to the left row eigenvector $\check{\boldsymbol{\nu}}(z,\tau)^{\mathsf{T}}$, modifies only every entry with index $j(s+1)$, $1 \leqslant j \leqslant k$. These are removed in the process of deflation; the scaling to obtain the basic deflated pencil removes the dependency on $\tau$. The first entry of the left eigenvector polynomial in (4.15) is one, thus we have proven that the polynomials (4.15) are eigenvector polynomials of the basic deflated pencil (4.14). □

We remark that we obtain the "natural" eigenvector polynomials if we scale the right eigenvector polynomial on the right of (4.15) by $h_{m,m-1}$.

**5. Pick your favorite pencil.** In the last section we proved that there are families of purified and deflated pencils, and showed by example how the normwise condition numbers of its constant eigenvalues differ. We introduced a new pencil, the

basic deflated pencil, which has only a mild and mostly implicit dependency on the seed values $\mu_j$, $1 \leqslant j \leqslant k$.

This offers much more flexibility: we can chose, depending on the application we have in mind, the appropriate type of pencil to compute eigenvalues. At the same time, we introduced more flexibility by adding a new parameter, the shift parameter $\tau$ in the families of deflated pencils. In the following list we gather all approaches and their properties.

**Sonneveld matrix:** Might be used if we are only interested in rough approximations to eigenvalues that are far from the selected seed values and rely on an existing code for Francis's (QR) algorithm, but do not have a code for the QZ algorithm at hand.

**Sonneveld pencil:** Might be used if we are only interested in eigenvalues that are far from the selected seed values.

**Purified pencil:** If we can select a shift parameter far form the seed values, but sufficiently far from infinity, the QZ algorithm or an adapted LZ algorithm gives good results. Numerical experiments suggest selecting a shift in the region of the converged eigenvalues.

**Deflated pencil:** As the shift just introduces a scaling, we ignore the family of deflated pencils and directly scale the basic deflated pencil blockwise using powers of two, such that the upper and lower blocks approximately have the same Frobenius norm. This removes the dependency on the shift parameter and gives good results using the QZ algorithm or an adapted LZ algorithm.

**Lanczos matrix:** At present this approach seems to be less stable than the others, but if we want to use Wilkinson's implicit double shift LR algorithm [37, p. 537] or Zhlobich's quasi-separable `dqds` [41], it might prove useful.

The QZ variants result in full pencils, the adapted LZ algorithms do not. If the pencils become large, which is an option, as they are computed by short recurrences, we might want to use an adapted LZ algorithm that preserves the banded structure. We could think of a variant based on a local strategy of pivoting, that only slowly destroys the banded structure. It remains to investigate the conditioning of LZ, LR, and `dqds` approaches.

## 6. Numerical experiments.

The numerical experiments in this section are used to show also the weaknesses of the approaches. For this reason we select a small $s$, in a real computation we would use a larger $s$. For the same reason we only use a well known academic toy example.

We present three examples. The first example shows that we can stably compute Ritz values for singular and almost singular pencils. The second example highlights the behaviour with respect to the shift parameter $\tau$. In the third example we compare the shifted pencils for a selected shift with the scaled basic deflated pencil.

### 6.1. The introductory example reconsidered.

We reconsider the numerical experiment underlying Figure 3.3. We chose as shift parameter $\tau = 2$. The resulting Figure 6.1 shows that even though the seed values come close to zero, we can stably compute Ritz values using an alternate purified pencil.

In Figure 6.2, we used the seed value zero throughout and the shift $\tau = 2$ in the alternate purified pencil. We remark that the standard purified pencil, i.e., the purified pencil we would obtain for the shift $\tau = 0$, is singular.

As we can see, the techniques introduced in §4 provide us with the countermeasures to cure the singular and almost singular pencils due to the seed value selection strategy at no extra cost. The same strategy works for the deflated pencils, which is not shown here. It remains to investigate the dependency on the shift parameter $\tau$; this task is treated in the next subsection.

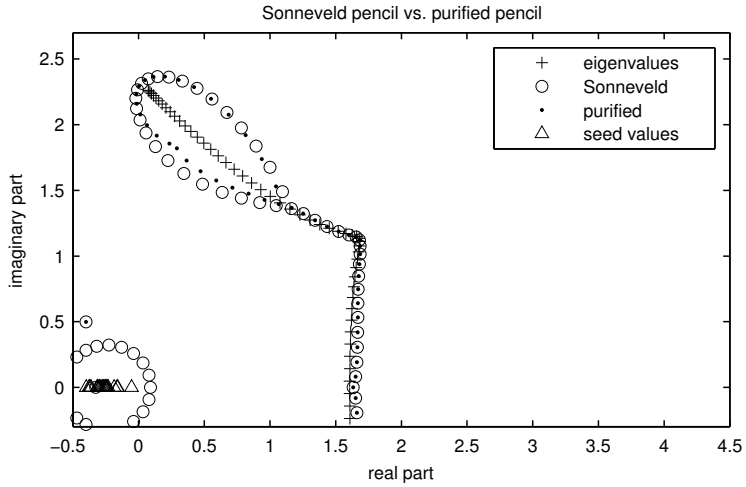


FIG. 6.1. *srIDR*(4) *for* $m = 124$ *steps on a Grcar matrix of size* $n = 100$*, different seed value selection scheme. Plus signs depict computed eigenvalues, triangles the seed values. Circles depict computed eigenvalues of the Sonneveld pencil, dots depict computed eigenvalues of the alternate purified pencil.*

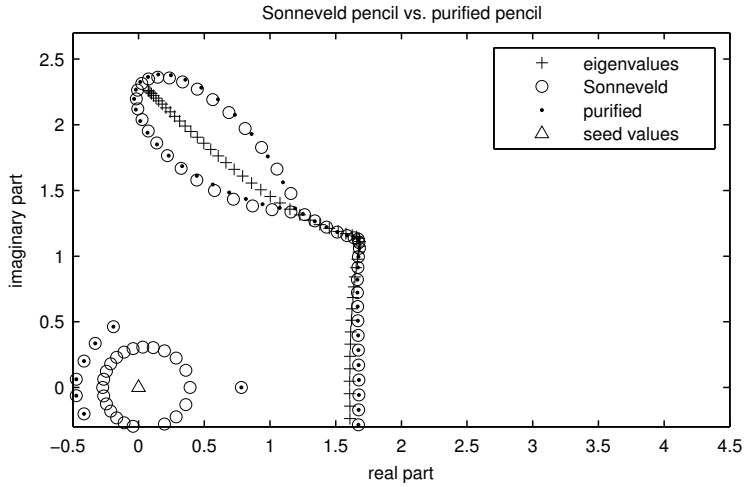


FIG. 6.2. *srIDR*(4) *for* $m = 124$ *steps on a Grcar matrix of size* $n = 100$*, zero seed value selection scheme. Plus signs depict computed eigenvalues, triangles the seed values. Circles depict computed eigenvalues of the Sonneveld pencil, dots depict computed eigenvalues of the alternate purified pencil.*

**6.2. The dependency on the shift parameter.** As a second example we used a Grcar matrix of size $n = 75$. We computed the matrices $\mathbf{H}_{103}$, $\mathbf{U}_{103}$ for mnelDR(3) with zero shift. The first figure of this example, Figure 6.3, shows the performance of the standard QZ algorithm on different pencils. All approximations are fairly good, differences are only visible for the eigenvalues with larger condition numbers. The Jordan block at zero of the Sonneveld pencil is approximated by a circle of Sonneveld Ritz values, close to this circle we observe seven ghost Ritz values that converge to these approximations and are found by all approaches. We (more or less randomly) selected the shift $\tau = 10$ for the purified pencil, the deflated pencil, and the Lanczos matrix.

In the second figure of the second example, Figure 6.4, we zoom into the picture and investigate the approximations close to the eigenvalue $\lambda \approx 0.2602 + 2.0778i$. Using variable precision with 100 digits, we computed the "exact" Ritz values, depicted with boxes in the first plot in the upper left corner. The exact Ritz values are really close

to the eigenvalues, which shows the effectiveness of Sonneveld methods for eigenvalue computations. In theory, all approximations coincide, what we observe is due to the finite precision computations and the structure of the pencils. In the upper right corner we plotted the 1000 nearest approximations obtained for equidistantly selected shifts $\tau$ in the interval $[5, 10]$ using the purified pencil; in the lower left corner we did the same for the deflated pencil; in the lower right corner we did the same for the Lanczos matrix. As we can see, the purified pencils and deflated pencils all give good approximations to the eigenvalue $\lambda \approx 0.2602 + 2.0778i$. In contrast, the Lanczos matrices give worse approximations, the spread is much larger than for the shifted pencils.

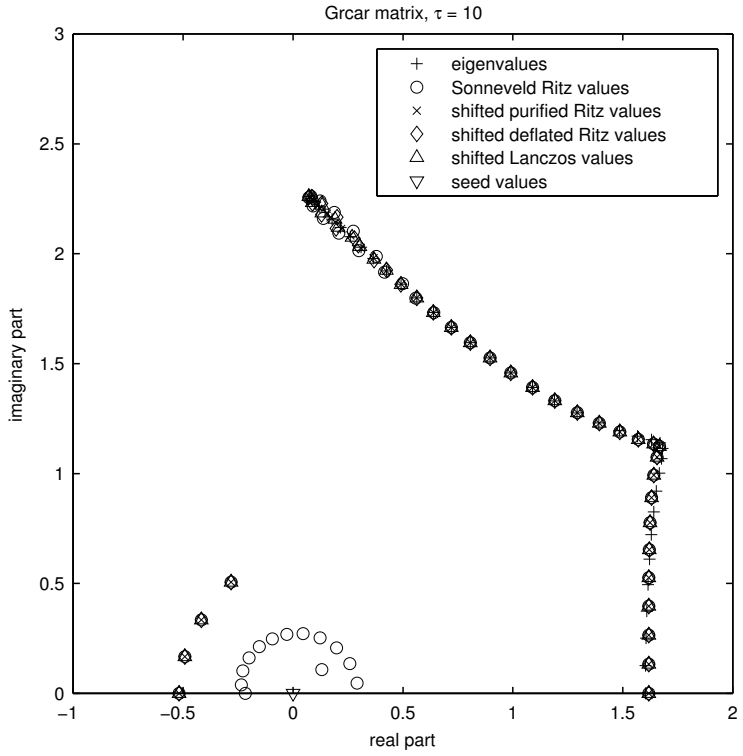


FIG. 6.3. *mnelIDR*(3) *for* $m = 103$ *steps on a Grcar matrix of size* $n = 75$*, zero seed value selection scheme. Plus signs depict computed eigenvalues, a lower triangle the seed value zero. Circles depict computed eigenvalues of the Sonneveld pencil, crosses those of the purified pencil for shift* $\tau = 10$*, diamonds those of the deflated pencil for shift* $\tau = 10$*, upper triangles those of the Lanczos matrix for shift* $\tau = 10$*.*

We conclude that the process of shifting to obtain an alternate purified or deflated pencil is only mildly dependent on the shift parameter: there are many shift values that can be used to obtain the Ritz values in a stable manner. This is supported by more numerical computations for a variety of matrices and seed value selection schemes not reported here.

**6.3. Using the scaled basic deflated pencil.** In this third example we use a Grcar matrix of size $n = 100$. The data stems from a run of $m = 152$ steps of mnelIDR(8) with zero shift strategy. We used a sort of over-scaling with powers of two such that the off-diagonal blocks become comparable in Frobenius norm. Figure 6.5 depicts the numerical approximations obtained using the Sonneveld pencil, the purified pencil and the deflated pencil, both with shift $\tau = 9$, and the scaled basic deflated pencil (4.14).

All approximations are of comparable quality. Repeating this experiment several times shows that only rarely one of the approaches turns out to be better than the others.

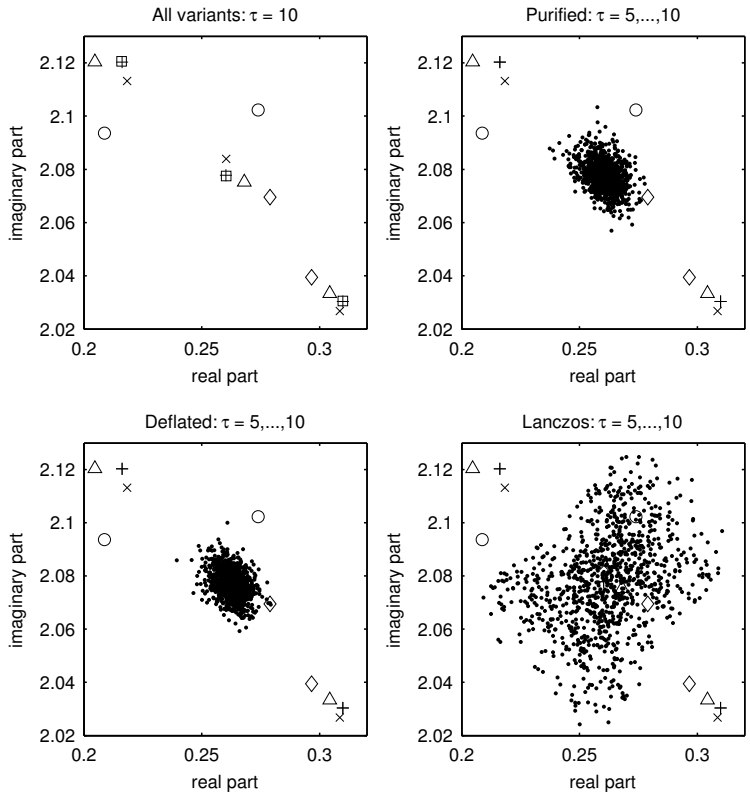


FIG. 6.4. *mneIDR*(3) *for* $m = 103$ *steps on a Grcar matrix of size* $n = 75$*, zero seed value selection scheme. All markers are as in Figure 6.3, except boxes in the top left figure, which denote the exact Ritz values, and dots in all other figures, which denote the Ritz value approximations for* 1000 *equidistant shifts in the interval* $[5, 10]$ *for the shifted purified pencils (top right), deflated pencils (bottom left), and Lanczos matrices (bottom right), respectively.*

**7. Conclusion & outlook.** In this note we presented ways to overcome instabilities in eigenvalue computations based on Sonneveld methods due to singular or badly conditioned pencils. The main results are the descriptions of the families of purified and deflated pencils in §4. It is hoped that this work helps in designing new, structurally adapted eigenvalue algorithms for the pencils arising in Sonneveld methods.

As any Hessenberg/upper triangular pencil defines a generalized Hessenberg decomposition, we might try to utilize these results in the development of adapted linear system solvers or eigenvector computations, which are both based on linear combinations of certain basis vectors. The explicit knowledge of the transitions is helpful in either developing recurrences for other sets of vectors, which might be used as basis vectors, or in the recomputation of coefficient vectors for the original basis. The latter can be used for 2-pass Sonneveld methods: firstly, the pencils are computed, discarding the basis vectors, secondly, after the coefficients of a linear combination of the basis vectors are known, we recompute the basis vectors and only update the wanted linear combinations.

**Acknowledgements.** The author would like to thank Beresford Parlett for persuading him to come to the 10th International Workshop on Accurate Solution of Eigenvalue Problems (IWASEP 10) in Dubrovnik; this note resulted from the preparation of my talk. He is very thankful to Reinaldo Astudillo, Marc Van Barel, Carla Ferreira, and Beresford Parlett for the interesting discussions & helpful input throughout the workshop.

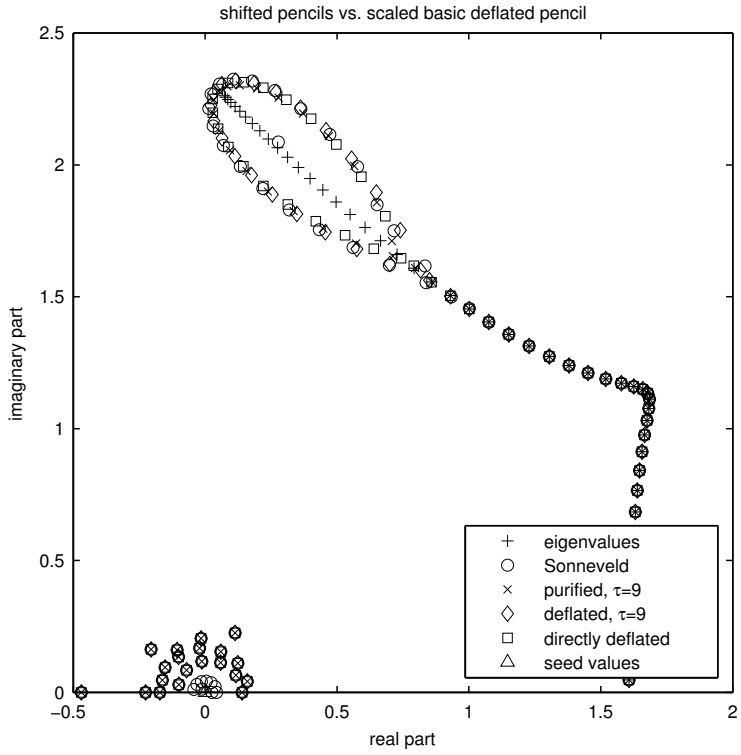


FIG. 6.5. *mneIDR*(8) *for* $m = 152$ *steps on a Grcar matrix of size* $n = 100$*, zero seed value selection scheme. All markers are as in Figure 6.3, the shift for the purified and the deflated pencil was* $\tau = 9$*. The boxes denote the numerical approximations obtained from the scaled basic deflated pencil defined in* (4.14).

## REFERENCES


[1] J. I. ALIAGA, D. L. BOLEY, R. W. FREUND, AND V. HERNÁNDEZ, *A Lanczos-type method for multiple starting vectors*, Math. Comp., (2000), pp. 1577–1601. [See page 2]

[2] W. E. ARNOLDI, *The principle of minimized iterations in the solution of the matrix eigenvalue problem*, Quart. Appl. Math., 9 (1951), pp. 17–29. [See page 2]

[3] R. ASTUDILLO AND M. B. VAN GIJZEN, *An induced dimension reduction algorithm to approximate eigenpairs of large nonsymmetric matrices*, AIP Conf. Proc., 1558 (2013), pp. 2277–2280. 11th International Conference of Numerical Analysis and Applied Mathematics 2013: ICNAAM 2013. [See page 6, 7]

[4] R. BEVILACQUA, E. BOZZO, AND G. M. DEL CORSO, *qd-type methods for quasiseparable matrices*, SIAM J. Matrix Anal. Appl., 32 (2011), pp. 722–747. [See page 9]

[5] J. DEMMEL AND B. KÅGSTRÖM, *The generalized Schur decomposition of an arbitrary pencil* $A - \lambda B$*: robust software with error bounds and applications. I. Theory and algorithms*, ACM Trans. Math. Software, 19 (1993), pp. 160–174. [See page 8]

[6] ———, *The generalized Schur decomposition of an arbitrary pencil* $A - \lambda B$*: robust software with error bounds and applications. II. Software and applications*, ACM Trans. Math. Software, 19 (1993), pp. 175–201. [See page 8]

[7] K. V. FERNANDO AND B. N. PARLETT, *Accurate singular values and differential qd algorithms*, Numer. Math., 67 (1994), pp. 191–229. [See page 8]

[8] C. FERREIRA, *The unsymmetric tridiagonal eigenvalue problem*, PhD thesis, University of Minho, 2007. [See page 8]

[9] C. FERREIRA AND B. PARLETT, *Real dqds for the nonsymmetric tridiagonal eigenvalue problem.* arXiv:1201.5065v1 [math.NA] 24 Jan 2012, 2012. [See page 8]

[10] G. FIX AND R. HEIBERGER, *An algorithm for the ill-conditioned generalized eigenvalue problem*, SIAM J. Numer. Anal., 9 (1972), pp. 78–88. [See page 8]

[11] J. G. F. FRANCIS, *The QR transformation: a unitary analogue to the LR transformation. I*, Comput. J., 4 (1961), pp. 265–271. [See page 6, 7]

[12] ———, *The QR transformation. II*, Comput. J., 4 (1962), pp. 332–345. [See page 6, 7]

[13] M. H. GUTKNECHT AND J.-P. M. ZEMKE, *Eigenvalue computations based on IDR*, SIAM J. Matrix Anal. Appl., 34 (2013), pp. 283–311. [See page 1, 2, 3, 4, 5, 10, 14]

[14] D. J. HIGHAM AND N. J. HIGHAM, *Structured backward error and condition of generalized eigenvalue problems*, SIAM J. Matrix Anal. Appl., 20 (1999), pp. 493–512 (electronic). [See

page 11, 12]
[15] L. Kaufman, *The LZ-algorithm to solve the generalized eigenvalue problem*, SIAM J. Numer. Anal., 11 (1974), pp. 997–1024. [See page 7, 8]
[16] C. B. Moler and G. W. Stewart, *An algorithm for generalized matrix eigenvalue problems*, SIAM J. Numer. Anal., 10 (1973), pp. 241–256. Collection of articles dedicated to the memory of George E. Forsythe. [See page 7]
[17] G. Peters and J. H. Wilkinson, *$Ax = \lambda Bx$ and the generalized eigenproblem*, SIAM J. Numer. Anal., 7 (1970), pp. 479–492. [See page 5]
[18] O. Rendel, A. Rizvanolli, and J.-P. M. Zemke, *IDR: a new generation of Krylov subspace methods?*, Linear Algebra Appl., 439 (2013), pp. 1040–1061. [See page 1, 2, 3, 5, 6, 9]
[19] O. Rendel and J.-P. M. Zemke, *On different basis expansions in Sonneveld methods*. unpublished draft, 2014. [See page 1, 3, 6]
[20] H. Rutishauser, *Der Quotienten-Differenzen-Algorithmus*, Z. Angew. Math. Physik, 5 (1954), pp. 233–251. [See page 8]
[21] ———, *Solution of eigenvalue problems with the LR-transformation*, Nat. Bur. Standards Appl. Math. Ser., 1958 (1958), pp. 47–81. [See page 8]
[22] ———, *Lectures on numerical mathematics*, Birkhäuser Boston Inc., Boston, MA, 1990. Edited by Martin Gutknecht with the assistance of Peter Henrici, Peter Läuchli and Hans-Rudolf Schwarz, with a foreword by Gutknecht and a preface by Henrici, Läuchli and Schwarz, Translated from the German and with a preface by Walter Gautschi. [See page 8]
[23] F. Schweins, *Theorie der Differenzen und Differentiale*, Verlag der Universitäts-Buchhandlung von C. F. Winter, Heidelberg, 1825. Digitized by Google, online available at http://books.google.de/books?id=dntNAAAAMAAJ. [See page 4]
[24] G. L. Sleijpen, P. Sonneveld, and M. B. van Gijzen, *Bi-CGSTAB as an induced dimension reduction method*, Appl. Numer. Math., 60 (2010), pp. 1100–1114. [See page 3]
[25] G. L. Sleijpen and M. B. van Gijzen, *Exploiting BiCGstab($\ell$) strategies to induce dimension reduction*, SIAM J. Sci. Comput., 32 (2010), pp. 2687–2709. [See page 1, 2, 3, 5, 9]
[26] G. L. G. Sleijpen and H. A. van der Vorst, *Maintaining convergence properties of BiCGstab methods in finite precision arithmetic*, Numer. Algorithms, 10 (1995), pp. 203–223. [See page 7]
[27] P. Sonneveld, *CGS, a fast Lanczos-type solver for nonsymmetric linear systems*, SIAM J. Sci. Statist. Comput., 10 (1989), pp. 36–52. [See page 3]
[28] ———, *On the convergence behavior of IDR($s$) and related methods*, SIAM J. Sci. Comput., 34 (2012), pp. A2576–A2598. [See page 2]
[29] P. Sonneveld and M. B. van Gijzen, *IDR($s$): A family of simple and fast algorithms for solving large nonsymmetric systems of linear equations*, SIAM J. Sci. Comput., 31 (2008), pp. 1035–1062. [See page 1, 3]
[30] D. C. Sorensen, *Implicit application of polynomial filters in a $k$-step Arnoldi method*, SIAM J. Matrix Anal. Appl., 13 (1992), pp. 357–385. [See page 6]
[31] M. Tanio and M. Sugihara, *GBi-CGSTAB($s, L$): IDR($s$) with higher-order stabilization polynomials*, J. Comput. Appl. Math., 235 (2010), pp. 765–784. [See page 1]
[32] H. A. van der Vorst, *Bi-CGSTAB: a fast and smoothly converging variant of Bi-CG for the solution of nonsymmetric linear systems*, SIAM J. Sci. Statist. Comput., 13 (1992), pp. 631–644. [See page 3]
[33] H. A. van der Vorst and P. Sonneveld, *CGSTAB, a more smoothly converging variant of CG-S*, Report 90-50, Department of Mathematics and Informatics, Delft University of Technology, 1990. [See page 3]
[34] M. B. van Gijzen, G. L. G. Sleijpen, and J.-P. M. Zemke, *Flexible and multi-shift induced dimension reduction algorithms for solving large sparse linear systems*, Numer. Linear Algebra Appl., (2014). doi: 10.1002/nla.1935. [See page 1, 7]
[35] M. B. van Gijzen and P. Sonneveld, *Algorithm 913: an elegant IDR($s$) variant that efficiently exploits biorthogonality properties*, ACM Trans. Math. Software, 38 (2011). [See page 1]
[36] P. Wesseling and P. Sonneveld, *Numerical experiments with a multiple grid and a preconditioned Lanczos type method*, in Approximation methods for Navier-Stokes problems (Proc. Sympos., Univ. Paderborn, Paderborn, 1979), R. Rautmann, ed., vol. 771 of Lecture Notes in Math., Berlin, Heidelberg, New York, 1980, Springer-Verlag, pp. 543–562. [See page 1, 3]
[37] J. H. Wilkinson, *The algebraic eigenvalue problem*, Clarendon Press, Oxford, 1965. [See page 8, 15]
[38] P. Wynn, *Continued fractions whose coefficients obey a noncommutative law of multiplication*, Arch. Rational Mech. Anal., 12 (1963), pp. 273–312. [See page 8]
[39] J.-P. M. Zemke, *Hessenberg eigenvalue-eigenmatrix relations*, Linear Algebra Appl., 414 (2006), pp. 589–606. [See page 10]
[40] F. Zhang, ed., *The Schur complement and its applications*, vol. 4 of Numerical Methods and Algorithms, Springer, New York, 2005. [See page 2]
[41] P. Zhlobich, *Differential qd algorithm with shifts for rank-structured matrices*, SIAM J. Matrix Anal. Appl., 33 (2012), pp. 1153–1171. [See page 8, 15]